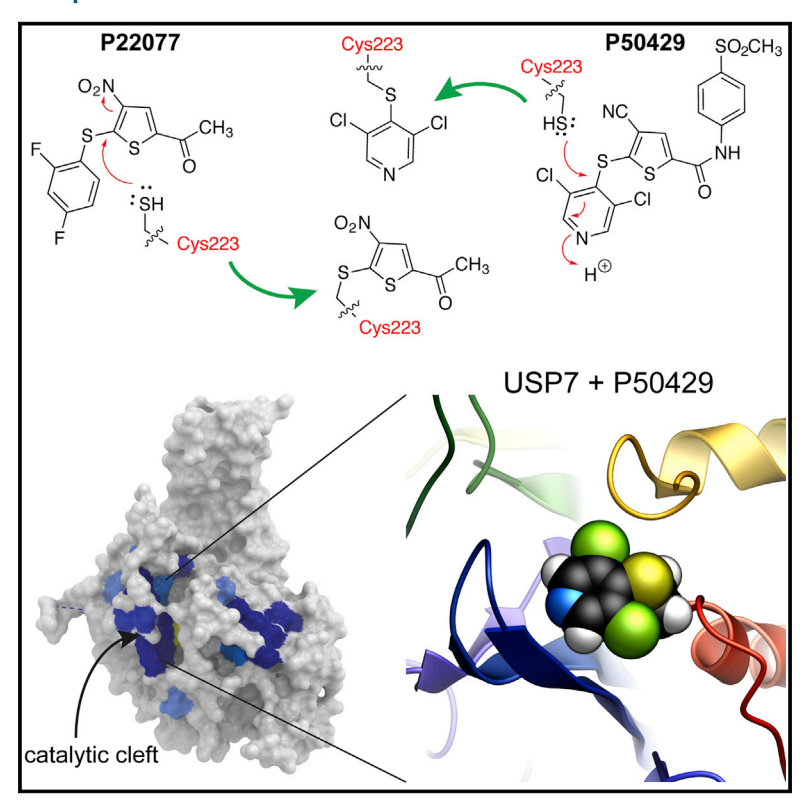
# **Cell Chemical Biology**

# **USP7-Specific Inhibitors Target and Modify the Enzyme's Active Site via Distinct Chemical Mechanisms**

# **Graphical Abstract**



# **Authors**

Alexandra Pozhidaeva, Gabrielle Valles, Feng Wang, ..., Jean Kanyo, Dennis Wright, Irina Bezsonova

# Correspondence

bezsonova@uchc.edu

# In Brief

Pozhidaeva et al. combine biophysical and biological methods to reveal the mechanism of action of two selective inhibitors of deubiquitinating enzyme USP7, and show that the compounds covalently and irreversibly modify the catalytic cysteine of the enzyme through distinct chemical reactions.

# **Highlights**

- Chemical mechanisms of USP7 inhibition by P22077 and P50429 are discovered
- The inhibitors covalently modify the active site of USP7
- The modifications induce conformational changes
- The compounds irreversibly and specifically inhibit USP7 in vitro and in cells





# USP7-Specific Inhibitors Target and Modify the Enzyme's Active Site via Distinct Chemical Mechanisms

Alexandra Pozhidaeva,<sup>1,5</sup> Gabrielle Valles,<sup>1</sup> Feng Wang,<sup>2</sup> Jian Wu,<sup>2</sup> David E. Sterner,<sup>2</sup> Phuong Nguyen,<sup>2</sup> Joseph Weinstock,<sup>2</sup> K.G. Suresh Kumar,<sup>2</sup> Jean Kanyo,<sup>3</sup> Dennis Wright,<sup>4</sup> and Irina Bezsonova<sup>1,6,\*</sup>

# **SUMMARY**

USP7 is a deubiquitinating enzyme that plays a pivotal role in multiple oncogenic pathways and therefore is a desirable target for new anti-cancer therapies. However, the lack of structural information about the USP7-inhibitor interactions has been a critical gap in the development of potent inhibitors. USP7 is unique among USPs in that its active site is catalytically incompetent, and is postulated to rearrange into a productive conformation only upon binding to ubiquitin. Surprisingly, we found that ubiquitin alone does not induce an active conformation in solution. Using a combination of nuclear magnetic resonance, mass spectrometry, computational modeling, and cell-based assays, we found that DUB inhibitors P22077 and P50429 covalently modify the catalytic cysteine of USP7 and induce a conformational switch in the enzyme associated with active site rearrangement. This work represents the first experimental insights into USP7 activation and inhibition and provides a structural basis for rational development of potent anti-cancer therapeutics.

#### INTRODUCTION

The ubiquitin proteasome system (UPS) is required for the tightly controlled degradation and turnover of the majority of the proteins in eukaryotic cells. Ubiquitination involves the enzymatic cascade of three classes of enzymes: E1 activating enzyme, E2 conjugating enzyme, and E3 ligase. These enzymes work together to ubiquitinate a protein substrate, targeting it for proteasomal degradation. The fate of a ubiquitinated protein can be reversed by deubiquitinating enzymes (DUBs), which remove ubiquitin chains from their substrates (Glickman and Ciechanover, 2002). Inhibiting components of the UPS reveals a promising therapeutic strategy to control cellular levels of proteins that lack enzymatic activity and thus cannot be inhibited (Buck-

ley and Crews, 2014). Because E3 ligases and DUBs directly interact with key proteins targeted for (de)ubiquitination and determine substrate specificity of UPS, their inhibition has emerged as a new approach to modulate stability of distinct proteins, including oncogenes and tumor suppressors (D'Arcy et al., 2015; Ndubaku and Tsui, 2015; Ronau et al., 2016).

Ubiquitin-specific protease 7 (USP7) is a cysteine protease that belongs to the USP family of DUBs (Everett et al., 1997). It is widely known for its central role in the DNA damage response pathway where it regulates protein levels of the tumor suppressor p53 in response to genotoxic stress (Li et al., 2002). In unstressed cells, USP7 preferably interacts with and stabilizes HDM2, an E3 ligase responsible for ubiquitinating p53 and targeting it for proteasomal degradation. During DNA damage, however, ATM-dependent phosphorylation of HDM2 reduces its affinity for USP7. As a consequence, USP7 is available to interact with p53, resulting in stabilization of p53 and initiation of the p53-dependent DNA damage response (Brooks et al., 2007; Hu et al., 2006; Li et al., 2004). In addition to p53, USP7 stabilizes key proteins involved in DNA replication, epigenetic DNA alterations, apoptosis, and cell-cycle control (Alonso-de Vega et al., 2014; Felle et al., 2011; Jagannathan et al., 2014; Luo et al., 2015; Meng et al., 2014; Oh et al., 2007; Zaman et al., 2013; Zhu et al., 2015; Zlatanou et al., 2015).

Microdeletions and mutations in the USP7 gene lead to neurodevelopmental disorders in humans characterized by intellectual disability, autism spectrum disorder, epilepsy, and hypogonadism (Hao et al., 2015), and dysregulation of USP7 expression has been reported in a number of human malignancies, including human prostate cancer (Song et al., 2008), ovarian cancer (Ma and Yu, 2016), and non-small-cell lung cancer (Masuya et al., 2006; Zhao et al., 2015). Furthermore, early studies in human colon cancer xenograft models showed that downregulation of USP7 suppresses cell proliferation and delays tumor growth due to p53 stabilization in the absence of cellular stress (Becker et al., 2008). The role of USP7 in oncogenesis and tumor suppression makes it an attractive pharmaceutical target for inhibition by small-molecule compounds (Nicholson and Suresh Kumar, 2011). High-throughput screening efforts led to the discovery of the first semi-specific, uncompetitive, and reversible inhibitor of USP7 (HBX 41,108), which was shown to stabilize



<sup>&</sup>lt;sup>1</sup>Department of Molecular Biology and Biophysics, UConn Health, Farmington, CT 06030, USA

<sup>&</sup>lt;sup>2</sup>Progenra Inc., Malvern, PA 19355, USA

<sup>&</sup>lt;sup>3</sup>Keck Foundation Biotechnology Resource Laboratory, Yale University, New Haven, CT 06511, USA

<sup>&</sup>lt;sup>4</sup>Department of Pharmaceutical Sciences, University of Connecticut, Storrs, CT 06268, USA

<sup>&</sup>lt;sup>5</sup>Present address: Department of Biochemistry and Molecular Biology, University of Massachusetts, Amherst, MA 01003, USA

<sup>&</sup>lt;sup>6</sup>Lead Contact

<sup>\*</sup>Correspondence: bezsonova@uchc.edu https://doi.org/10.1016/j.chembiol.2017.09.004

p53 and inhibit cell growth in HCT116 colon cancer cells (Colland et al., 2009). Later, additional USP7 compounds with increased specificity were reported (Reverdy et al., 2012) along with a family of dual USP7/USP47 inhibitors (compounds 1–14) (Weinstock et al., 2012). Inhibition of USP7 by P5091 (compound 1) was shown to cause apoptosis of multiple myeloma cells and prolonged survival in animal xenograft models (Chauhan et al., 2012). Further optimization of P5091 led to the discovery of P22077 (compound 4), which inhibited neuroblastoma growth (Fan et al., 2013), and P50429 (compound 14), which inhibited the proliferation of HCT116 cells (Weinstock et al., 2012). Although all of the above compounds show antitumor properties in various cancer cell lines and animal models, none are very potent and all require further optimization.

USP7 consists of an N-terminal substrate binding TRAF-like domain, five C-terminal regulatory ubiquitin-like (UBLs) domains, and a central catalytic core that binds ubiquitin and removes it from the substrate (Faesen et al., 2011; Holowaty et al., 2003; Zapata et al., 2001). The catalytic domain of USP7 adopts a papain protease-like fold that binds ubiquitin. This fold contains Thumb, Palm, and extended Fingers regions similar to those of other USPs (Hu et al., 2002; Molland et al., 2014). The region of the catalytic domain that is targeted by USP7-specific inhibitors remains unknown. Furthermore, given the structural conservation of the catalytic domains within the family of 58 USP enzymes, it is not clear how specificity for USP7 can be achieved (Nijman et al., 2005).

In this study we uncover the mechanism of USP7 inhibition by two small-molecule compounds and provide new insights into the mechanism of the enzyme activation.

#### **RESULTS**

# Nuclear Magnetic Resonance Studies of 41 kDa Catalytic Core of USP7 in Solution

Structural information about a protein target and its interaction with small-molecule compounds is the key for successful rational drug design and optimization. Although several crystal structures are available for the catalytic core of USP7 and USP7-ubiquitin complexes (PDB: 1NB8, 1NBF, and 4M5W) (Hu et al., 2002; Molland et al., 2014), structures of the enzyme with any known inhibitors have not been obtained. The relatively large size of the catalytic domain (41 kDa) has also hindered its investigation in solution. We have overcome this hurdle by using full-protein deuteration in combination with TROSY-based nuclear magnetic resonance (NMR) experiments designed for large biological systems (Pervushin et al., 1997). A <sup>1</sup>H-<sup>15</sup>N TROSY spectrum displayed good signal dispersion indicative of well-structured domains (Figure S1). The quality of the NMR data facilitated backbone resonance assignment, prerequisite for mapping of inhibitor binding sites.

Sequential assignment using a standard triple-resonance NMR approach was achieved for a total of 83% of the backbone atoms (NH, CO, C $\alpha$ , and C $\beta$ ), with 81% of amides assigned (Figure 1A). The absence of several peaks and the presence of weak peaks prevented a higher percentage of resonance assignments. In particular, 61 of the 343 non-proline residues' resonances could not be identified in the  $^1\text{H}-^{15}\text{N}$  TROSY spectrum. About one-half of the missing signals correspond to residues

located in  $\beta$  strands ( $\beta$ 8,  $\beta$ 10, and  $\beta$ 11), which are a part of an antiparallel  $\beta$  sheet buried in the interior of the protein. The absence of these signals is likely explained by the difficulty of  $^2$ H/ $^1$ H exchange in the hydrophobic core of USP7. Another cluster of missing resonances belongs to N-terminal residues 217–227. This region contains C223, one of three residues of the catalytic triad of USP7 (C223, H464, and D481). Overall, the stability and behavior of the USP7 catalytic domain in solution indicate that it is well suited for probing USP7-ligand interactions by NMR.

# Interaction of the USP7 Catalytic Core with Ubiquitin

The catalytic domain of USP7 binds ubiquitin, while its TRAF-like and UBL domains specifically recognize its ubiquitinated substrates. The USP7 catalytic core was previously crystallized alone and with ubiquitin aldehyde, which covalently links ubiquitin to the catalytic C223 of USP7. A comparison of the two structures revealed dramatic rearrangement of the USP7 active site and surrounding loops when bound to ubiquitin (Hu et al., 2002; Molland et al., 2014). The apoenzyme remained catalytically incompetent with its catalytic triad (C223, H464, and D481) misaligned (PDB: 1NB8, 4M5X, and 4M5W); however, the ubiquitin-linked enzyme adopted a catalytically competent conformation (PDB: 1NBF), suggesting that ubiquitin binding induces activation of the enzyme. A similar interaction with free ubiquitin could not be confirmed by surface plasmon resonance experiments, suggesting that the interaction is very weak (Faesen et al., 2011). We used NMR, which is sensitive to weak and transient interactions (O'Connell et al., 2009) to detect USP7/ubiquitin binding in solution and follow the anticipated structural changes. As seen in Figure 1B, the <sup>1</sup>H-<sup>15</sup>N TROSY spectrum of the USP7 catalytic domain displays gradual shifts in NMR resonance positions for a number of peaks upon titration with ubiquitin, indicative of a direst interaction between the two molecules with the exchange between free and bound states fast on the NMR timescale. Per-residue chemical shift perturbations,  $\Delta \omega,$  calculated as the distance between the free and bound peaks are presented in Figure 1C and Table S1.

The gradual chemical shift changes in the <sup>1</sup>H-<sup>15</sup>N TROSY spectrum facilitated quantification of USP7-ubiquitin binding affinity and mapping of the ubiquitin binding site on the surface of USP7. As seen in Figure 1C, addition of ubiquitin causes prominent peak perturbations for a number of USP7 residues, with peaks of Y331, K378, R343, D346, Q371, Q372, A381, Q387, and V393 exhibiting shifts over 100 Hz (0.125 <sup>1</sup>H ppm). The NMR titration curve fits a two-state binding model (Figure 1E), confirming that the USP7 catalytic domain binds ubiquitin with low affinity ( $K_D = 105.7 \pm 15.9 \mu M$ ). NMR chemical shift mapping revealed that the residues most sensitive to binding are located in  $\beta$  strands  $\beta$ 1,  $\beta$ 2,  $\beta$ 4,  $\beta$ 5,  $\beta$ 6, and  $\beta$ 7. This region forms the ubiquitin binding fingers of the USP7 catalytic domain (Figure 1D), consistent with the crystal structure of the domain in complex with ubiquitin aldehyde (PDB: 1NBF) (Hu et al., 2002). Surprisingly, the anticipated chemical shift perturbations of the active site and its surrounding loops, such as blocking loop 1 (BL1, residues 407-429), blocking loop 2 (BL2, residues 458-465), and switching loop (SL, residues 283-295), which rearrange during activation to accommodate ubiquitin tail, were not observed (Figures 1C and S2B). These results show that,

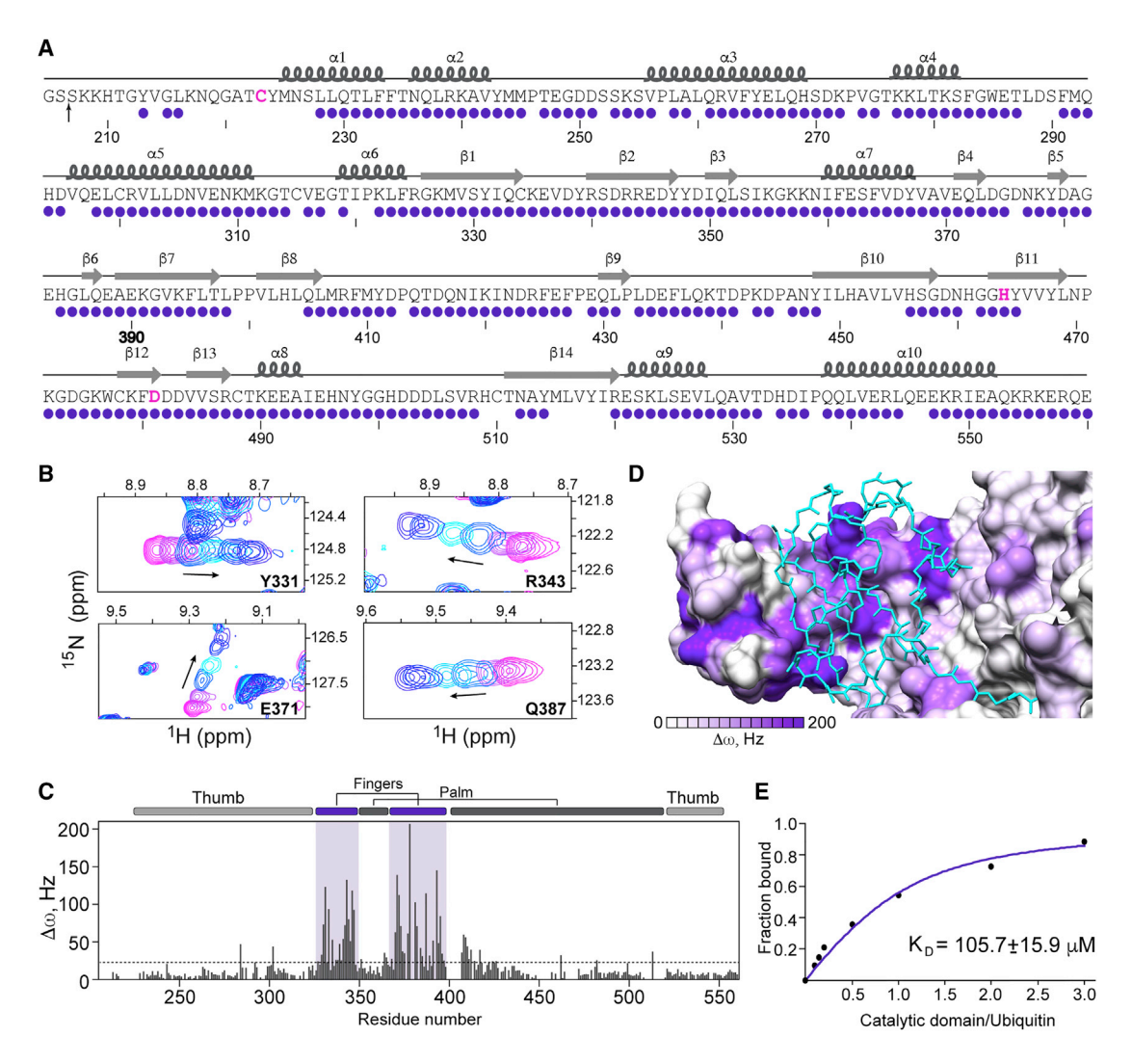


Figure 1. Isolated USP7 Catalytic Domain Binds Ubiquitin

(A) Sequence-specific NMR chemical shift assignment of the catalytic domain. Purple dots signify assigned residues. Secondary structure elements are labeled, residues of the catalytic triad are shown in pink.

- (B) NMR chemical shift perturbations, Δω, in <sup>1</sup>H-<sup>15</sup>N TROSY spectra of the catalytic domain caused by addition of increasing amounts of ubiquitin (1:3 molar ratio). (C) A plot of per-residue Δω between free and ubiquitin-bound states of USP7.
- (D) Surface representation of the ubiquitin binding region of USP7 colored according to  $\Delta\omega$ . Ubiquitin is shown in cyan.
- (E) A plot of normalized global  $\Delta\omega$  as a function of catalytic domain to ubiquitin ratio used to estimate the  $K_D$  of binding. See also Figures S1 and S2.

unlike ubiquitin aldehyde, the C terminus of free ubiquitin does not enter the catalytic cleft and ubiquitin interaction alone does not cause the active site rearrangement necessary for catalysis as was previously believed.

# **Mapping of the Small-Molecule Binding Site**

The USP7/USP47 inhibitors P22077 and P50429 are analogs of P5091, a lead compound that showed antitumor potential in cancer cell lines and mice xenograft models (Chauhan et al., 2012; Weinstock et al., 2012). Both inhibitors are trisubstituted thiophenes with 5-(2,4-difluorophenyl)thio, 4-nitro, and 2-acetyl substituents in P22077, and 5-(3,5-dichloropyridyl)thio, 4-cyano, and 2-(4-(methylsulfonyl)phenyl)-NH substituents in P50429. P50429 exhibits 20-fold more potent inhibition of USP7 compared with P22077 (half maximal inhibitory concentra-

tion = 0.42 versus  $8.0~\mu\text{M}$ ) (Weinstock et al., 2012). To structurally characterize the binding of P22077 and P50429 to USP7 we performed NMR titrations in which increasing amounts of each compound were gradually added to the  $^2\text{H}/^{15}\text{N}/^{12}\text{C}$ -labeled catalytic domain. Despite limited solubility of both inhibitors in water, sufficient amounts of the inhibitors remained in solution to cause significant (20–120 Hz or 0.025–0.15  $^1\text{H}$  ppm) chemical shift perturbations in  $^1\text{H}-^{15}\text{N}$  TROSY spectra of USP7 (lower panels in Figures 2A and 2B and Tables S2 and S3). As a result of the interaction, intensity of several NMR peaks of free USP7 gradually decrease, and new peaks corresponding to the bound state gradually appear in a new position of the spectrum. This gradual progression, exemplified by the T280 peak in the upper panel of Figures 2A and 2B, is characteristic for a slow on the NMR timescale exchange between free and inhibitor-bound

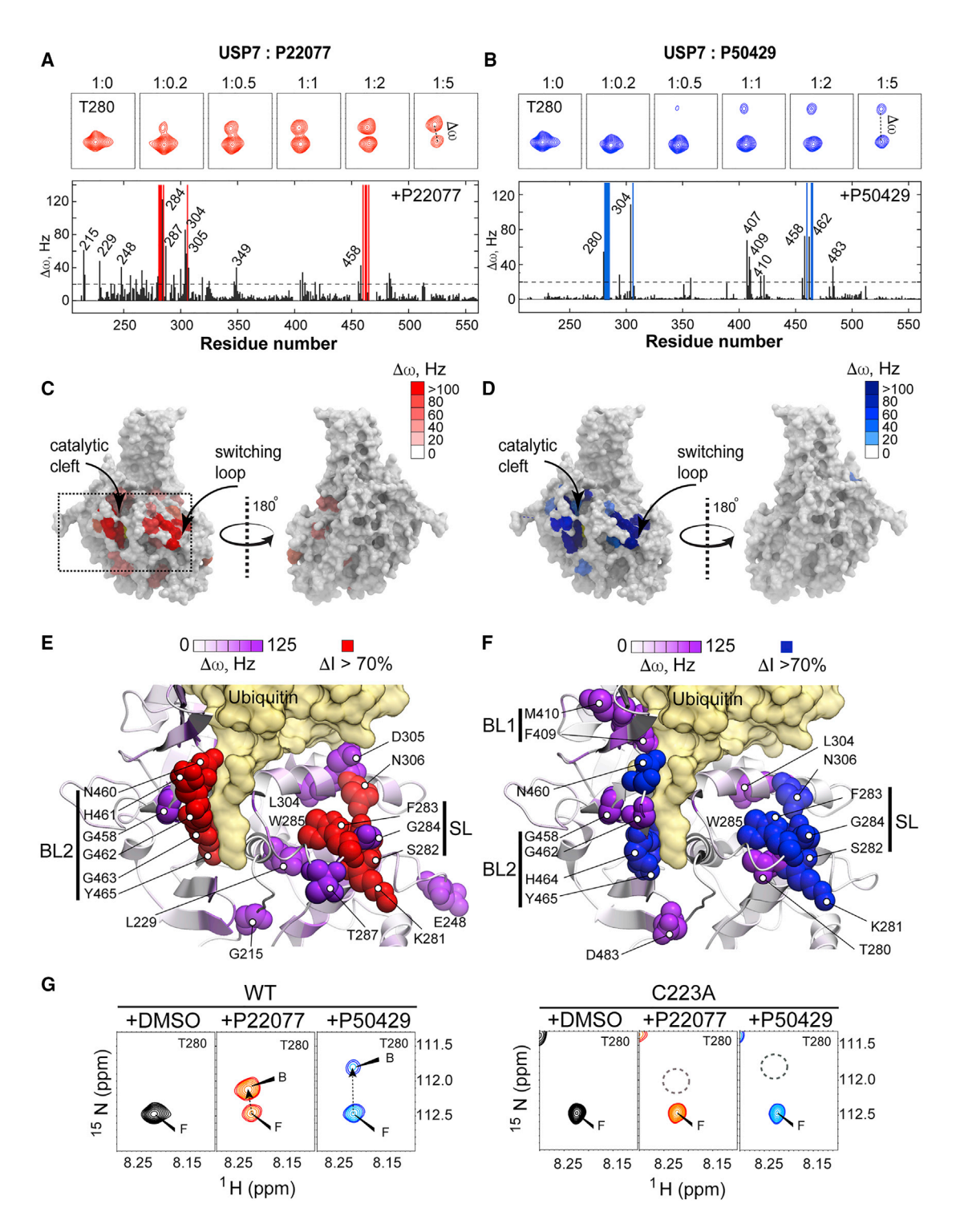


Figure 2. NMR Mapping of the Inhibitors Binding Site on the Structure of USP7

(A and B) A plot of per-residue NMR chemical shift perturbations,  $\Delta\omega$ , caused by addition of 5-molar excess of inhibitors P22077 (A) and P50429 (B) to USP7. Top panel shows gradual changes in a select region of USP7  $^1$ H- $^{15}$ N TROSY spectrum upon titration. Values of  $\Delta\omega$  > 20 Hz are considered significant, residues with largest perturbations ( $\Delta\omega$  > 40 Hz for P22077 and  $\Delta\omega$  > 30 Hz for P50429) are labeled.  $\Delta\omega$  of residues sensitive to the inhibitors with chemical shifts assigned only in "free" state are arbitrarily set to 140 Hz to reflect significant chemical shift perturbation (red and blue bars).

(C and D) Inhibitor binding site mapping. Surface representation of USP7 structure (PDB: 4M5W) colored according to  $\Delta\omega$  induced by either P22077 (red) or P50429 (blue). Each representation is shown in two orientations.

(E and F) Inhibitor-induced  $\Delta\omega$  mapped on the structure of USP7 active site in complex with ubiquitin (PDB: 1NBF). USP7 is shown as a ribbon colored by  $\Delta\omega$  (purple). Residues with largest  $\Delta\omega$  are shown as spheres. Residues with chemical shifts assigned only in "free" state are shown in red (E) and

states of the USP7. Remarkably, the free peaks are still visible at the last titration point, suggesting that saturation was not reached in the titrations, likely due to limited solubility of the compounds.

Per-residue chemical shift perturbations caused by P22077 and P50429 are shown in Figures 2A and 2B, where residues with largest  $\Delta \omega$  are labeled. For several residues largely perturbed by the compounds,  $\Delta\omega$  could not be accurately estimated because their "bound" state resonances could not be unambiguously assigned. Those were arbitrary set to 140 Hz to indicate large perturbations. These residues are shown as red and blue bars in Figures 2A and 2B, and as red and blue spheres in Figures 2E and 2F. Chemical shift perturbations of more than 20 Hz were considered significant and were mapped onto the structure of USP7 catalytic domain. Chemical shift mapping revealed that residues sensitive to addition of either of the two DUB inhibitors cluster in two regions on the surface of the protein that are separated by a stretch of unassigned N-terminal residues, including catalytic cysteine (Figures 2C and 2D). Both inhibitors largely affect BL2 and SL, which form the catalytic cleft and switch conformation upon enzyme activation (Hu et al., 2002; Molland et al., 2014). In addition, P50429 uniquely affect residues 407 and 409-410, which constitute BL1 (Figures 2E and 2F). These results suggest that P22077 and P50429 may target the active site of the enzyme. Interestingly, the area perturbed by the inhibitors is large relative to the size of the compounds, suggesting that the binding may also induce conformational changes around the active site. Remarkably, the affected residues are located in the three aforementioned major areas (BL1, BL2, and SL) that undergo structural rearrangement during enzyme activation.

# Mechanism of USP7 Inhibition by DUB Inhibitors P22077 and P50429

The presence of a doubly deactivated, highly electron-deficient thiophene ring in both of the USP7 inhibitors used in this study suggested that the molecules might react directly with nucleophilic residues, such as cysteine, thus leading to covalently modified adducts. To investigate whether these compounds bind USP7 reversibly, or covalently modify the protein, we performed intact protein mass spectrometry (MS) analysis of free and inhibitor-treated catalytic domain (Figure 3A), followed by liquid chromatography-tandem mass spectrometry (LC-MS/MS) experiments on tryptically digested samples (Figures 3B and 3C). The LC-MS spectrum of the free catalytic domain showed a major peak with an average mass of 52,966.15 Da, which corresponds to the expected MW of the SUMO-tagged USP7 catalytic domain construct used in this experiment. The intact masses of both complexes with the inhibitors were greater than that of the free protein, suggesting that both compounds covalently modify USP7. These experiments were reproduced using catalytic domain of USP7 without SUMO tag (Figure S4A). Observed mass shifts of 169.29 and 146.004 Da for P22077 and P50429, respectively, are smaller than the corresponding molecular weights of the compounds (315.322 Da for P22077, 484.411 Da for P50429), suggesting that significant parts of the small molecules are lost during final modification of the enzyme.

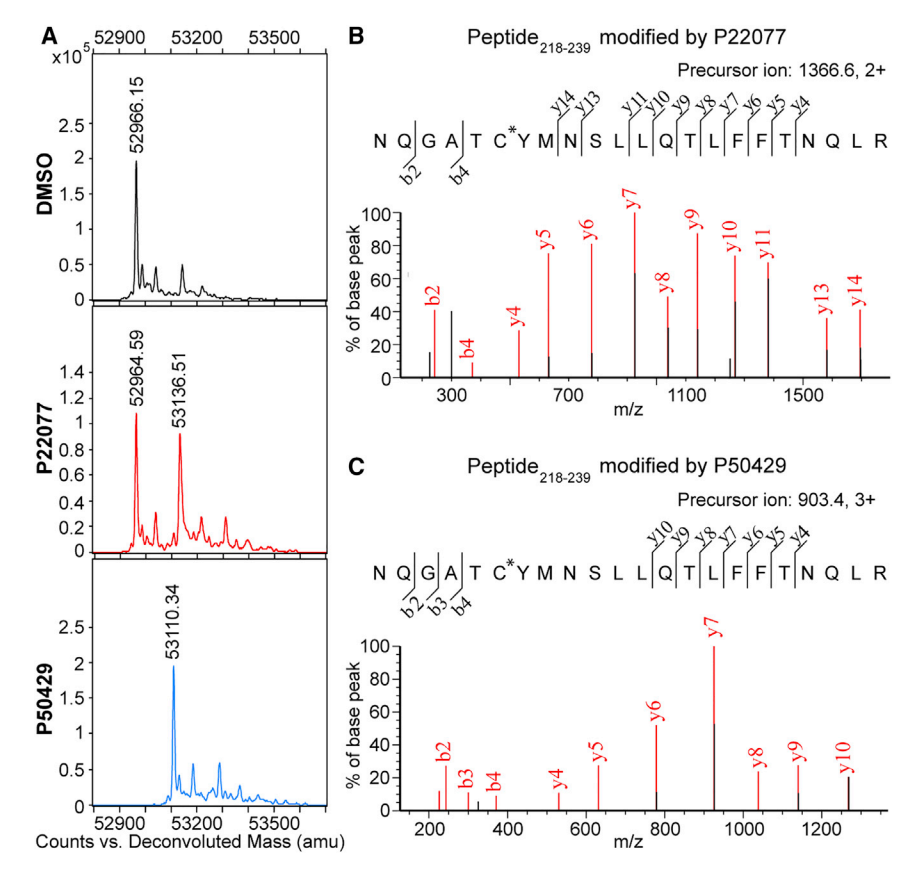
To investigate whether these compounds covalently modify the catalytic and/or other cysteine residues within USP7, we have treated the catalytic domain with 5-molar excess of the inhibitors for ~24 hr and performed LC-MS/MS experiments on tryptically digested samples, as described in the STAR Methods. A variable modification of cysteine was configured for each inhibitor based on the added net mass determined by the intact mass study. Over 90% of the protein sequence coverage was achieved for the free and inhibitor-treated protein samples, including all seven cysteine residues. Virtually all identified tryptic peptides 218-239 from samples treated with either P22077 or P50429 exhibited mass shifts of 169 and 146 Da, respectively, compared with the same peptide from the unmodified protein (Figures 3B and 3C). Importantly, the residue harboring the modification was almost exclusively assigned to catalytic C223. The data for P50429 was remarkably clear cut, with every peptide encompassing C223 identified as containing the inhibitor-based modification, while peptides containing other cysteine residues were rarely identified as modified. The putative 169 Da adduct for P22077 was more promiscuous, with C223 modified in all but one instance, and other cysteines occasionally

To further confirm that C223 is the target of the inhibitors *in vitro* we have introduced a C223A mutation. NMR spectra of the mutant confirm that C223A remains well folded in solution. NMR titrations of the mutant with the inhibitors show that C223A completely abrogates binding to both inhibitors (Figures 2G and S3). Furthermore, LS-MS analysis of the C223A mutant treated with 20-fold molar excess of either inhibitor for 4 hr reveals no evidence of adduct formation (Figure S4D).

Altogether, the MS results in combination with mutagenesis and NMR-based mapping of the binding site strongly suggest that both of the compounds occupy the active site of the USP7 catalytic domain and selectively covalently modify the catalytic C223 residue, thus irreversibly blocking USP7's enzymatic activity. Figure 4 shows the proposed mechanisms of modification by the inhibitors. The observed mass shift of 169 Da for the P22077modified protein is consistent with an average molecular weight of 1-(4-nitro-thiophen-2-yl)-ethanone group (3 in Figure 4). The mass shift of 146 Da in the case of P50429 corresponds to an average molecular weight of the 3,5-dichloropyridyl group of the molecule (7 in Figure 4). Element composition of the proposed modifications was supported by analysis of the MS/ MS isotope patterns (Figures S4B and S4C). Therefore, despite the overall scaffold structural similarity of the compounds (Weinstock et al., 2012), each compound modified the USP7 catalytic core in a unique manner. P22077 (1) transfers the central thiophene onto the catalytic cysteine through a postulated mechanism involving initial nucleophilic attack on the thiophene to give an intermediate thio-orthoester (2) which collapses

blue (F).  $\Delta I > 70\%$ , "free" peak intensity loss over 70%; BL1, blocking loop 1; BL2, blocking loop 2; SL, switching loop. Ubiquitin is shown as beige surface.

<sup>(</sup>G) C223A mutation of USP7 prevents P22077 and P50429 binding. A select region of wild-type (WT) and C223A NMR spectrum, as in (A), is shown in the presence of DMSO (black), P22077 (red), and P50429 (blue). Both "free" (F) and "bound" (B) T280 peaks are visible in the spectra of WT treated with the inhibitors, while only "free" peaks are observed in C223A. Dashed circles signify the missing peaks. The full spectra for WT and C223A USP7 are shown in Figure S3.



through expulsion of difluorothiophenol (4) to form the re-aromatized adduct (3). Although P50429 (5) is also poised for a similar substitution reaction, the enzymatic reaction follows a different course as a result of the substitution of the phenyl ring in (1) for the pyridyl ring in (5), which renders the ring prone to nucleophilic attack. A similar addition/elimination process occurs through the intermediacy of (6) to transfer the pyridyl ring to the enzyme as in (7), with the thiophenyl moiety (8) serving as the leaving group. The inhibitor's specificity toward C223 is likely enhanced by basic H464 which deprotonates C223 making it more reactive than typical surface thiols.

# Inhibition of Endogenous Full-Length USP7 by DUB Inhibitors P22077 and P50429 in Jurkat Cells

To determine whether USP7 inhibition by P22077 and P50429 is also achieved against full-length USP7 in the context of live cells, we pre-treated Jurkat cells with either DMSO or graded concentrations of the compounds for 4 hr, and monitored the activity of immunoprecipitated USP7 using a Ub-CHOP2 reporter assay. As seen in Figure 5A, both compounds showed dose-dependent inhibition of USP7 catalytic activity, with strong inhibition at a dose of 10  $\mu M$ . Notably, total DUB activity measured in cell lysates was not significantly affected by these inhibitors (Figure S5A), indicating their cellular selectivity, in agreement with previously published results (Altun et al., 2011; Weinstock et al., 2012). Furthermore, treatment of HEK293T cells with either P22077 or P50429 prevented labeling of the USP7 catalytic domain with Ub-vinyl methyl ester (Ub-VME) probe, a ubiquitin variant known to covalently bind the catalytic cysteine of DUBs

#### Figure 3. Inhibitors P22077 and P50429 Covalently Modify Catalytic C223 of the USP7 Active Site In Vitro

(A) Deconvoluted mass spectra of SUMO-tagged USP7 catalytic domain treated *in vitro* for 4 hr with either DMSO (black) or 20-fold molar excess of inhibitors P22077 (red) and P50429 (blue). Average intact masses of the significant peaks are shown.

(B) MS/MS spectrum of peptide corresponding to residues 218–239 modified by P22077 (m/z = 1,366.6 [M+2H]<sup>2+</sup>).

(C) MS/MS spectrum of the same peptide modified by P50429 ( $m/z=903.4~[{\rm M}+3{\rm H}]^{3+}$ ). The b-ions denote N-terminal fragment ions and y-ions represent C-terminal fragment ions. Ions matched to the peptide sequence are shown in red.

Catalytic C223 is marked with an asterisk. See also Figure S4.

(Borodovsky et al., 2002). Consistent with results of USP7 activity assays and former studies (Weinstock et al., 2012), more potent P50429 completely abrogated conjugation of USP7 with UbVME, while P22077 inhibited the labeling only partially (Figure S5B).

The cellular effect of USP7 inhibition was also assessed by monitoring levels of its known protein targets. We used western blotting of Jurkat cell lysates to

evaluate the effect of P22077 and P50429 on the stability of DNA methyltransferase DNMT1 and E3 ligase UHRF1 (Felle et al., 2011), both essential for maintenance of genomic DNA methylation, as well as HDM2. Compared with cells treated with DMSO, treatment with either compound resulted in dose-dependent decreases for all three substrates (Figure 5D). Thus, these compounds not only inhibit the isolated catalytic domain *in vitro* but also effectively inhibit full-length USP7 in cells, as demonstrated by the destabilization of USP7 substrates.

# Inhibition of USP7 by DUB Inhibitors P22077 and P50429 Is Irreversible in Cells

To verify that the proposed inhibition mechanism is valid in cells we have tested whether USP7 is inhibited irreversibly when cells are treated with P22077 and P50429. For this we pre-treated HCT116 cells with DMSO, P22077, or P50429, blocked new protein synthesis, and measured USP7 activity after 24 hr (Figure 5B). We found that USP7 activity does not recover in the absence of new protein synthesis, and USP7 remains inactive 24 hr post-treatment, consistent with the irreversible inhibition.

To confirm the proposed adduct formation in cells, HEK293T cells expressing the catalytic domain of USP7 were treated with DMSO, P22077, or P50429. The catalytic domain was then purified and analyzed using MS. As seen in Figure 5C, treatment of cells with P22077 results in 169 Da adduct formation, and treatment with P50429 adds 146 Da to the mass of the intact USP7 catalytic domain. Notably, the adduct sizes found in cells are identical to those found *in vitro* (Figures 3A and S4A), in

Figure 4. Proposed Mechanisms of Chemical Reaction between C223 of USP7 and Inhibitors P22077 and P50429 P22077 and P50429 reactions are shown on top and bottom, respectively. C223 is the catalytic cysteine of USP7.

agreement with the proposed reaction mechanisms (Figure 4). Furthermore, according to MS analysis, the C223A mutant of USP7 shows no evidence of adduct formation in cells (Figure 5C), confirming that catalytic C223 is preferably targeted by P22077 and P50429 not only *in vitro* but also in cells.

#### **DISCUSSION**

Dysregulation of the UPS has been reported in multiple human pathologies. Thus, targeting the UPS is considered a promising therapeutic strategy to treat cancer, cardiovascular, neurodegenerative, and immunological disorders. Two US Food and Drug Administration-approved proteasome inhibitors, bortezamib and carfilzomib, are currently used for treatment of multiple myeloma (Kouroukis et al., 2014; Meng et al., 1999). More recently, other components of the UPS, such as E2-conjugating enzymes, E3 ligases, and DUBs have been exploited as potential targets for drug discovery. Inhibition of USP7 is of special interest because of its role in turnover of multiple proteins involved in DNA replication and repair, epigenetic regulation of gene transcription, immune responses, and cell-cycle control. Here we report the first structural and mechanistic insights into USP7 inhibition by small-molecule compounds.

By assigning NMR resonances of the catalytic domain of USP7, we developed a powerful tool for studying this challenging dynamic system in solution. We have shown that even transient and short-lived interactions of USP7 can now be detected, along with evidence of conformational dynamics. Specifically, our NMR studies of the binding between the catalytic domain and ubiquitin revealed that, contrary to previous reports, this interaction alone is not sufficient for active site rearrangement. According to the crystal structures, binding of ubiquitin to USP7 causes realignment of the catalytic triad into a catalytically competent state that is associated with structural changes in BL1, BL2, and SL regions of the protein (Figures 2E and 2F). These conformational changes are required to accommodate the C terminus

of ubiquitin in the active site of the enzyme (Hu et al., 2002; Molland et al., 2014). In contrast, our results show that residues involved in such rearrangement are not sensitive to ubiquitin binding in solution. Specifically, no significant chemical shift changes were induced by ubiquitin in the active site, or residues located in BL1, BL2, or SL (Figures 1C and S2). This indicates that the C-terminal tail of isolated ubiquitin does not enter the catalytic cavity in solution. We hypothesize that the active conformation of USP7 captured in the crystal structure (Hu et al., 2002) is induced by the covalent attachment of ubiquitin to the catalytic cysteine of USP7, which irreversibly traps the C-terminal tail of ubiquitin inside the catalytic cleft. Other domains of this multi-domain protein likely play a role in its activation (Faesen et al., 2011; Rouge et al., 2016). Moreover, the presence of a ubiquitinated substrate may ensure proper positioning of the isopeptide bond between ubiquitin and the substrate inside the catalytic cleft. The importance of the ubiquitinated substrate for the enzyme's activation suggests that targeting the USP7 substrate binding sites may provide an effective and highly specific approach to inhibiting USP7 in the future.

To investigate the molecular mechanism of USP7 inhibition, we identified a binding site for two USP7/USP47-specific DUB inhibitors, P22077 and P50429, on the structure of USP7. A combination of NMR, MS, and mutagenesis revealed that both inhibitors target the active site of USP7 and covalently modify C223. Remarkably, unlike free ubiquitin, which fails to activate the enzyme, the inhibitors perturb residues in BL1, BL2, and SL, precisely the regions of USP7 that change conformation during active site rearrangement (Hu et al., 2002; Molland et al., 2014). These findings also highlight the significance of the interaction between the ubiquitin flexible tail and the active site for realignment of the latter. The inhibitors appear to mimic this interaction, causing conformational changes in the active site.

The catalytic domain of USP7 contains seven cysteines, four of them surface exposed and, therefore, have a potential of being modified by reactive small-molecule compounds. Strikingly,

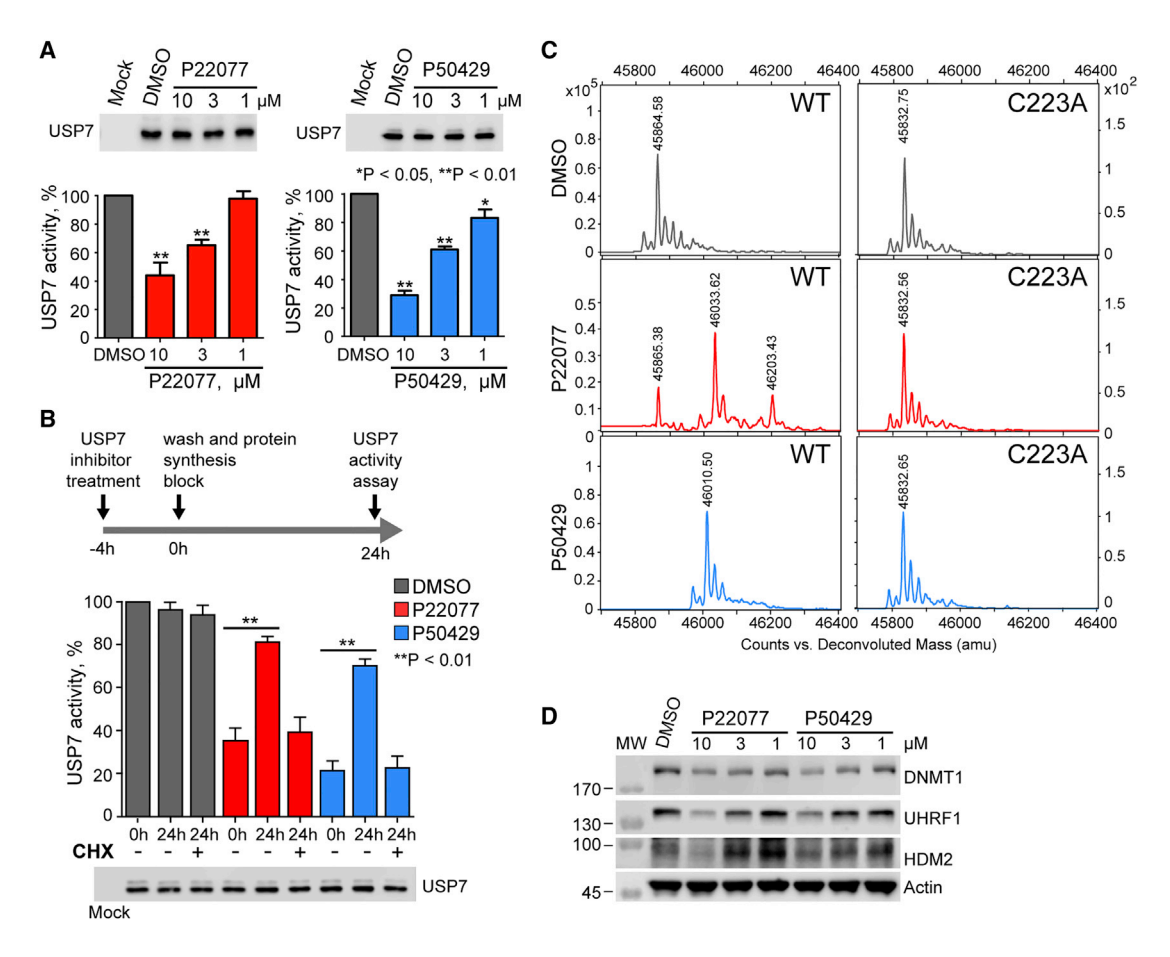


Figure 5. P22077 and P50429 Target the Active Site of USP7 and Irreversibly Inhibit Its Activity in Cells

(A) Concentration-dependent inhibition of endogenous USP7 by P22077 and P50429 in cells. Jurkat cells were treated with DMSO or compounds at indicated concentrations for 4 hr; USP7 was isolated by immunoprecipitation (IP) and its activity measured in the Ub-CHOP2-based activity assay. Activity of USP7 from either DMSO- (control) or inhibitor-treated cells plotted as percent of the control activity (mean  $\pm$  SD). \*p < 0.05 and \*\*p < 0.01 versus DMSO-treated cells. (B) USP7 inhibition by P22077 and P50429 is irreversible in mammalian cells. HCT116 cells were pre-treated with DMSO, P22077, or P50429 for 4 hr, washed with 1 × PBS to remove the excess compounds, followed by CHX treatment to block new protein synthesis (top). Recovery of USP7 activity was measured 24 hr later in the presence and absence of new protein production.

(C) LC-MS spectrum of WT and C223A USP7 catalytic domain isolated from HEK293T cells that were treated with 50  $\mu$ M of P22077 (red), P50429 (blue), or DMSO (black) for 4 hr. Average intact masses of the significant peaks are shown.

(D) Dose-dependent downregulation of USP7 substrates. Endogenous levels of USP7 substrates DNMT1, UHRF1, and HDM2 monitored in Jurkat cells pretreated with either DMSO or the compounds at indicated concentrations for 24 hr. Actin serves as a loading control. See also Figure S5.

we found that both compounds modify only the catalytic C223. This result is further confirmed by C223A mutation, which abrogates interaction with and modification of USP7 both in vitro and in cells. The molecular scaffold of the compounds allows for specific binding, and the presence of doubly deactivated thiophene leads to modification of C223 situated at the bottom of the catalytic cleft. The reaction is possible due to the realignment of the active site upon inhibitor binding, which results in deprotonation of the cysteine thiol group by catalytic H464. Notably, although both compounds are chemically similar and possess the basic structure of a trisubstituted thiophene, MS experiments revealed that unique substructures of each inhibitor had been transferred to the protein and indicated an intriguing divergence in the reactivity profile of the two inhibitors (Figure 4). The preference for attack on the pyridine in P50429 may relate to either reduced electrophilicity of its thiophene relative to the thiophene in P22077 (nitro/acetyl versus cyano/carboxamido)

or a more optimal trajectory for attack in the bound state. Figures 6A and 6B depict C223 modified by compounds P22077 and P50429. In general, the docked poses of thiophene and pyridyl rings are similar. The rings have hydrophobic interactions with surrounding residues Y224, M292, and F409, and an electrostatic interaction with H456. The only hydrogen bond is between the oxygen atom within the acetyl group and the alpha-hydrogen atom of G462 (Figure 6A). Notably, as both reactions proceed through a nucleophilic aromatic substitution reaction to deliver an S-arylated cysteine, the adducts are likely much more stable than those formed from more reversible Michael-type reactions on deactivated alkenes and, therefore, are expected to produce a longer duration of inhibition.

MS data in combination with cell biology assays confirmed that the proposed chemical mechanism of USP7 inhibition by P22077 and P50429 (Figure 4) is valid both *in vitro* and in mammalian cells (Figure 5). Full-length USP7 is a large (1,102)

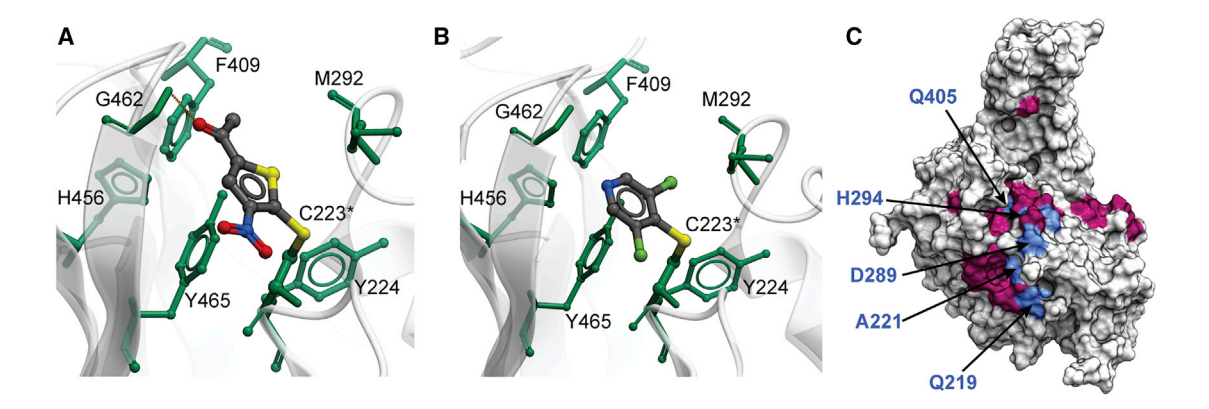


Figure 6. Specificity Determinants of Dual USP7/USP47 Inhibitors
(A and B) Covalent docking models of the USP7 active site modified by P22077 (A) and P50429 (B). Catalytic C223 is marked with an asterisk.
(C) Surface representation of the USP7 catalytic domain with conserved among USPs residues shown in maroon. Residues unique to USP7 and USP47 are shown in blue.

amino acid residues) protein consisting of seven domains proposed to adopt a compact conformation during the enzyme activation (Faesen et al., 2011), which may interfere with the inhibitor binding. Here, we showed that both compounds inhibit the catalytic activity of endogenous full-length USP7. Furthermore, treatment of cells with P22077 and P50429 results in formation of C223 adducts identical to those observed *in vitro*. Overall, P50429 proved to have more potency against USP7, in agreement with previous studies (Weinstock et al., 2012).

Stabilization of p53, along with growth arrest of tumor cells, are well-known effects of USP7 inhibition (Chauhan et al., 2012; Colland et al., 2009; Reverdy et al., 2012). However, it was suggested that p53-independent pathways might also be involved in the cytotoxic effects of the USP7 inhibitors (Chauhan et al., 2012). UHRF1 and DNMT1, recently discovered substrates of USP7, are critical for maintenance of genomic DNA methylation during replication (Felle et al., 2011). Therefore, we explored the effect of P22077 and P50429 on the stability of UHRF1, DNMT1, and HDM2 in Jurkat cells. The dose-dependent decreases in the levels of all three substrates suggests that their stability is compromised by deubiquitination. While degradation of HDM2 leads to stabilization of p53, the degradation of UHRF1 and DNMT1 might cause methylation defects in newly synthetized DNA. These downstream effects may contribute to the overall cytotoxic activity of these compounds.

USP7 belongs to a superfamily of USP cysteine proteases consisting of 58 proteins with structurally conserved catalytic cores, which makes development of USP7-specific inhibitors challenging. Indeed, the two compounds tested in this work are the most specific among the currently available USP7 inhibitors; however, they both can inhibit USP7 and its close homolog USP47 (Love et al., 2007). The fact that inhibitors P22077 and P50429 bind to the conserved catalytic cleft of USP7 is intriguing and raises the question of how the specificity is achieved. In an effort to address this question, we performed protein sequence alignment using PROMALS3D (Pei et al., 2008), followed by calculation of conservation score (ConSurf) (Ashkenazy et al., 2010) for a set of USP enzymes that are selectively inhibited by P22077 (USP7 and USP47), as well as enzymes USP2, 4, 5, 8, 9X, 15, 20, and 28, not susceptible to inhibition by P22077 (Altun

et al., 2011). As expected, the majority of the residues in the catalytic cavity are highly conserved (Figure 6C). However, a few residues are uniquely conserved in USP7 and USP47 and varied in other USPs. Specifically, Q219 of USP7 is present only in USP47, while other USPs contain a hydrophobic amino acid residue at the equivalent position. Acidic amino acid residues equivalent to D289 in USP7 are also found in USP47 (E246), but replaced by neutral residues in USP2, 4, 5, 8, 9X, 15, and 28, and by basic R in USP20. In addition, the positively charged H294 in USP7 is conserved in USP47 and USP9X, in contrast to Q at the equivalent position in all other analyzed USPs. The hydrophobic side chain of USP7 A221, which is near the catalytic C223, is preserved in USP47 (M175) and USP9X (A1564) but changed to polar N in others. Finally, Q405 in USP7 is conserved among USP47, USP9X, and USP5. Other proteins have H at the equivalent positions, with the exception of USP28, which has D. Overall, although some of these residues are not unique for USP7 and USP47, only these two enzymes contain all five. This distinct residue combination creates a network of hydrophobic and electrostatic interactions unique to the active sites of USP7 and USP47, which may provide the basis for the observed specificity of inhibitors.

Alternatively, it is possible that USP7-specific inhibitors preferentially target its unique, misaligned active site for initial binding. Indeed, catalytic triads in all other known USP structures are found in the catalytically competent conformation, even in the absence of ubiquitin (Avvakumov et al., 2006; Clerici et al., 2014; Hu et al., 2005; Komander et al., 2008). In this light, the structure of the catalytic core of USP47 also inhibited by P22077 and P50429 is a subject of great interest.

Altogether, our results reveal the molecular mechanisms of USP7 inhibition by P22077 and P50429. We showed that inhibitors specifically bind to the catalytic cleft of the enzyme and subsequently modify the catalytic C223. The modification of the cysteine thiol group irreversibly inhibits the enzymatic activity of USP7 by preventing formation of anionic sulfur and its subsequent nucleophilic attack on the C-terminal carbonyl carbon of ubiquitin. Previously, only X-ray crystallography was used to structurally characterize the catalytic domains of USP proteins. We have shown that these large enzymes can be successfully

studied in solution. Such studies may provide a unique insight into dynamic conformational changes and transient interactions within the molecule. More importantly, these studies will facilitate compound optimization and the discovery of more potent and specific inhibitors of USP7 and other pharmacologically important USPs.

#### **SIGNIFICANCE**

Inactivation of USP7 has recently emerged as a new approach to treatment of multiple human malignancies. However, the lack of structural information about the USP7-inhibitor interactions has been a critical gap in the development of specific and potent USP7 inhibitors. Here, we report the first structural analysis of USP7 inhibition with two small-molecule compounds. We demonstrate that both inhibitors specifically target the catalytic cleft of the enzyme and covalently modify C223 of the active site via distinct chemical mechanisms. Detailed knowledge of the mechanism of USP7 inhibition will allow rational design of improved inhibitors as the basis of a new class of anti-cancer therapeutics.

#### **STAR**\*METHODS

Detailed methods are provided in the online version of this paper and include the following:

- KEY RESOURCES TABLE
- CONTACT FOR REAGENT AND RESOURCE SHARING
- EXPERIMANTAL MODEL AND SUBJECT DETAILS
  - Bacterial Strains
  - Cell Lines
- METHOD DETAILS
  - USP7 Inhibitors
  - Protein Expression and Purification
  - NMR Spectroscopy
  - Mass Spectrometry
  - Protein Ligand Docking
  - O Immunoprecipitation and DUB Activity Measurements
  - Irreversible Inhibition of Endogenous USP7 in HCT116 Cells
  - Western Blotting
  - Ub-VME based USP7 Activity Assay
- DATA AND SOFTWARE AVAILABILITY

# SUPPLEMENTAL INFORMATION

Supplemental Information includes five figures and three tables and can be found with this article online at https://doi.org/10.1016/j.chembiol.2017. 09.004.

#### **AUTHOR CONTRIBUTIONS**

A.P. and I.B. conceived the experiments. A.P. performed and analyzed most of the NMR experiments and wrote the manuscript. A.P. and I.B. performed computational molecular docking. G.V. performed and analyzed C223A NMR experiments. J. Weinstock designed USP7 inhibitors used in the study. J. Wu synthesized the inhibitors. K.G.S.K. designed the cellular experiments. F.W. and P.N. performed and analyzed cellular experiments. F.W. performed *in vitro* and cellular protein LC-MS experiments. D.S. performed cloning of

mammalian and bacterial expression constructs. J.K. performed LC-MS/MS experiments, and J.K. and A.P. analyzed the results. D.W. proposed the chemical mechanism of USP7 inhibition. J.K., K.G.S.K., J. Weinstock, G.V., and I.B. reviewed and edited the manuscript.

#### **ACKNOWLEDGMENTS**

We thank N. Rauniyar for his help with MS data collection and analysis, SGC Toronto for providing a plasmid of USP7, D. Korzhnev, S. Weller, J. Radolf, and K. Hadden for critical reading of the manuscript. I.B. is supported by NSF award 1616184. F.W., J. Wu., D.E.S., P.N., J. Weinstock, and K.G.S.K. are employees of Progenra Inc.

Received: December 5, 2016 Revised: June 24, 2017 Accepted: September 12, 2017 Published: October 19, 2017

#### REFERENCES

Alonso-de Vega, I., Martin, Y., and Smits, V.A. (2014). USP7 controls Chk1 protein stability by direct deubiquitination. Cell Cycle *13*, 3921–3926.

Altun, M., Kramer, H.B., Willems, L.I., McDermott, J.L., Leach, C.A., Goldenberg, S.J., Kumar, K.G., Konietzny, R., Fischer, R., Kogan, E., et al. (2011). Activity-based chemical proteomics accelerates inhibitor development for deubiquitylating enzymes. Chem. Biol. *18*, 1401–1412.

Ashkenazy, H., Erez, E., Martz, E., Pupko, T., and Ben-Tal, N. (2010). ConSurf 2010: calculating evolutionary conservation in sequence and structure of proteins and nucleic acids. Nucleic Acids Res. *38*, W529–W533.

Avvakumov, G.V., Walker, J.R., Xue, S., Finerty, P.J., Jr., Mackenzie, F., Newman, E.M., and Dhe-Paganon, S. (2006). Amino-terminal dimerization, NRDP1-rhodanese interaction, and inhibited catalytic domain conformation of the ubiquitin-specific protease 8 (USP8). J. Biol. Chem. *281*, 38061–38070.

Becker, K., Marchenko, N.D., Palacios, G., and Moll, U.M. (2008). A role of HAUSP in tumor suppression in a human colon carcinoma xenograft model. Cell Cycle *7*, 1205–1213.

Borodovsky, A., Ovaa, H., Kolli, N., Gan-Erdene, T., Wilkinson, K.D., Ploegh, H.L., and Kessler, B.M. (2002). Chemistry-based functional proteomics reveals novel members of the deubiquitinating enzyme family. Chem. Biol. 9, 1149–1159.

Brooks, C.L., Li, M., Hu, M., Shi, Y., and Gu, W. (2007). The p53-Mdm2-HAUSP complex is involved in p53 stabilization by HAUSP. Oncogene 26, 7262-7266.

Buckley, D.L., and Crews, C.M. (2014). Small-molecule control of intracellular protein levels through modulation of the ubiquitin proteasome system. Angew. Chem. Int. Ed. 53, 2312–2330.

Chauhan, D., Tian, Z., Nicholson, B., Kumar, K.G., Zhou, B., Carrasco, R., McDermott, J.L., Leach, C.A., Fulcinniti, M., Kodrasov, M.P., et al. (2012). A small molecule inhibitor of ubiquitin-specific protease-7 induces apoptosis in multiple myeloma cells and overcomes bortezomib resistance. Cancer Cell *22*, 345–358.

Clerici, M., Luna-Vargas, M.P., Faesen, A.C., and Sixma, T.K. (2014). The DUSP-Ubl domain of USP4 enhances its catalytic efficiency by promoting ubiquitin exchange. Nature Commun. 5, 5399.

Colland, F., Formstecher, E., Jacq, X., Reverdy, C., Planquette, C., Conrath, S., Trouplin, V., Bianchi, J., Aushev, V.N., Camonis, J., et al. (2009). Small-molecule inhibitor of USP7/HAUSP ubiquitin protease stabilizes and activates p53 in cells. Mol. Cancer Ther. 8, 2286–2295.

D'Arcy, P., Wang, X., and Linder, S. (2015). Deubiquitinase inhibition as a cancer therapeutic strategy. Pharmacol. Ther. 147, 32–54.

Delaglio, F., Grzesiek, S., Vuister, G.W., Zhu, G., Pfeifer, J., and Bax, A. (1995). NMRPIPE - a multidimensional spectral processing system based om UNIX pipes. J. Biomol. NMR 6, 277–293.

Everett, R.D., Meredith, M., Orr, A., Cross, A., Kathoria, M., and Parkinson, J. (1997). A novel ubiquitin-specific protease is dynamically associated with the

PML nuclear domain and binds to a herpesvirus regulatory protein. EMBO J. 16. 1519–1530.

Faesen, A.C., Dirac, A.M., Shanmugham, A., Ovaa, H., Perrakis, A., and Sixma, T.K. (2011). Mechanism of USP7/HAUSP activation by its C-terminal ubiquitin-like domain and allosteric regulation by GMP-synthetase. Mol. Cell *44*, 147–159.

Fan, Y.H., Cheng, J., Vasudevan, S.A., Dou, J., Zhang, H., Patel, R.H., Ma, I.T., Rojas, Y., Zhao, Y., Yu, Y., et al. (2013). USP7 inhibitor P22077 inhibits neuroblastoma growth via inducing p53-mediated apoptosis. Cell Death Dis. 4. e867.

Felle, M., Joppien, S., Nemeth, A., Diermeier, S., Thalhammer, V., Dobner, T., Kremmer, E., Kappler, R., and Langst, G. (2011). The USP7/Dnmt1 complex stimulates the DNA methylation activity of Dnmt1 and regulates the stability of UHRF1. Nucleic Acids Res. 39, 8355–8365.

Glickman, M.H., and Ciechanover, A. (2002). The ubiquitin-proteasome proteolytic pathway: destruction for the sake of construction. Physiol. Rev. 82, 373–428.

Hao, Y.H., Fountain, M.D., Jr., Fon Tacer, K., Xia, F., Bi, W., Kang, S.H., Patel, A., Rosenfeld, J.A., Le Caignec, C., Isidor, B., et al. (2015). USP7 acts as a molecular rheostat to promote WASH-dependent endosomal protein recycling and is mutated in a human neurodevelopmental disorder. Mol. Cell *59*, 956–969.

Holowaty, M.N., Sheng, Y., Nguyen, T., Arrowsmith, C., and Frappier, L. (2003). Protein interaction domains of the ubiquitin-specific protease, USP7/HAUSP. J. Biol. Chem. 278, 47753–47761.

Hu, M., Li, P., Li, M., Li, W., Yao, T., Wu, J.W., Gu, W., Cohen, R.E., and Shi, Y. (2002). Crystal structure of a UBP-family deubiquitinating enzyme in isolation and in complex with ubiquitin aldehyde. Cell *111*, 1041–1054.

Hu, M., Li, P., Song, L., Jeffrey, P.D., Chenova, T.A., Wilkinson, K.D., Cohen, R.E., and Shi, Y. (2005). Structure and mechanisms of the proteasome-associated deubiquitinating enzyme USP14. EMBO J. 24, 3747–3756.

Hu, M., Gu, L., Li, M., Jeffrey, P.D., Gu, W., and Shi, Y. (2006). Structural basis of competitive recognition of p53 and MDM2 by HAUSP/USP7: implications for the regulation of the p53-MDM2 pathway. PLoS Biol. 4, e27.

Jagannathan, M., Nguyen, T., Gallo, D., Luthra, N., Brown, G.W., Saridakis, V., and Frappier, L. (2014). A role for USP7 in DNA replication. Mol. Cell. Biol. *34*, 132–145.

Komander, D., Lord, C.J., Scheel, H., Swift, S., Hofmann, K., Ashworth, A., and Barford, D. (2008). The structure of the CYLD USP domain explains its specificity for Lys63-linked polyubiquitin and reveals a B box module. Mol. Cell 29, 451–464.

Kouroukis, T.C., Baldassarre, F.G., Haynes, A.E., Imrie, K., Reece, D.E., and Cheung, M.C. (2014). Bortezomib in multiple myeloma: systematic review and clinical considerations. Curr. Oncol. *21*, e573–603.

Li, M., Chen, D., Shiloh, A., Luo, J., Nikolaev, A.Y., Qin, J., and Gu, W. (2002). Deubiquitination of p53 by HAUSP is an important pathway for p53 stabilization. Nature *416*, 648–653.

Li, M., Brooks, C.L., Kon, N., and Gu, W. (2004). A dynamic role of HAUSP in the p53-Mdm2 pathway. Mol. Cell 13, 879–886.

Love, K.R., Catic, A., Schlieker, C., and Ploegh, H.L. (2007). Mechanisms, biology and inhibitors of deubiquitinating enzymes. Nat. Chem. Biol. 3, 697–705

Luo, M., Zhou, J., Leu, N.A., Abreu, C.M., Wang, J., Anguera, M.C., de Rooij, D.G., Jasin, M., and Wang, P.J. (2015). Polycomb protein SCML2 associates with USP7 and counteracts histone H2A ubiquitination in the XY chromatin during male meiosis. PLoS Genet. *11*, e1004954.

Ma, M., and Yu, N. (2016). Ubiquitin-specific protease 7 expression is a prognostic factor in epithelial ovarian cancer and correlates with lymph node metastasis. Onco Targets Ther. 9, 1559–1569.

Malakhov, M.P., Mattern, M.R., Malakhova, O.A., Drinker, M., Weeks, S.D., and Butt, T.R. (2004). SUMO fusions and SUMO-specific protease for efficient expression and purification of proteins. J. Struct. Funct. Genomics  $5,\,75$ –86.

Masuya, D., Huang, C., Liu, D., Nakashima, T., Yokomise, H., Ueno, M., Nakashima, N., and Sumitomo, S. (2006). The HAUSP gene plays an important

role in non-small cell lung carcinogenesis through p53-dependent pathways. J. Pathol. 208, 724–732.

Meng, L., Mohan, R., Kwok, B.H., Elofsson, M., Sin, N., and Crews, C.M. (1999). Epoxomicin, a potent and selective proteasome inhibitor, exhibits in vivo antiinflammatory activity. Proc. Natl. Acad. Sci. USA *96*, 10403–10408

Meng, H., Harrison, D.J., and Meehan, R.R. (2014). MBD4 interacts with and recruits USP7 to heterochromatic foci. J. Cell. Biochem. *116*, 476–485.

Molland, K., Zhou, Q., and Mesecar, A.D. (2014). A 2.2 A resolution structure of the USP7 catalytic domain in a new space group elaborates upon structural rearrangements resulting from ubiquitin binding. Acta Crystallogr. F Struct. Biol. Commun. 70, 283–287.

Ndubaku, C., and Tsui, V. (2015). Inhibiting the deubiquitinating enzymes (DUBs). J. Med. Chem. 58, 1581–1595.

Neves, M.A., Totrov, M., and Abagyan, R. (2012). Docking and scoring with ICM: the benchmarking results and strategies for improvement. J. Comput. Aided Mol. Des. 26, 675–686.

Nicholson, B., and Suresh Kumar, K.G. (2011). The multifaceted roles of USP7: new therapeutic opportunities. Cell Biochem. Biophys. 60, 61–68.

Nijman, S.M., Luna-Vargas, M.P., Velds, A., Brummelkamp, T.R., Dirac, A.M., Sixma, T.K., and Bernards, R. (2005). A genomic and functional inventory of deubiquitinating enzymes. Cell *123*, 773–786.

O'Connell, M.R., Gamsjaeger, R., and Mackay, J.P. (2009). The structural analysis of protein-protein interactions by NMR spectroscopy. Proteomics 9, 5224–5232

Oh, Y.M., Yoo, S.J., and Seol, J.H. (2007). Deubiquitination of Chfr, a check-point protein, by USP7/HAUSP regulates its stability and activity. Biochem. Biophys. Res. Commun. *357*, 615–619.

Pei, J., Kim, B.H., and Grishin, N.V. (2008). PROMALS3D: a tool for multiple protein sequence and structure alignments. Nucleic Acids Res. *36*, 2295–2300

Pervushin, K., Riek, R., Wider, G., and Wuthrich, K. (1997). Attenuated T2 relaxation by mutual cancellation of dipole-dipole coupling and chemical shift anisotropy indicates an avenue to NMR structures of very large biological macromolecules in solution. Proc. Natl. Acad. Sci. USA *94*, 12366–12371.

Pettersen, E.F., Goddard, T.D., Huang, C.C., Couch, G.S., Greenblatt, D.M., Meng, E.C., and Ferrin, T.E. (2004). UCSF Chimera – a visualization system for exploratory research and analysis. J. Comput. Chem. *25*, 1605–1612.

Reverdy, C., Conrath, S., Lopez, R., Planquette, C., Atmanene, C., Collura, V., Harpon, J., Battaglia, V., Vivat, V., Sippl, W., et al. (2012). Discovery of specific inhibitors of human USP7/HAUSP deubiquitinating enzyme. Chem. Biol. *19*, 467–477.

Ronau, J.A., Beckmann, J.F., and Hochstrasser, M. (2016). Substrate specificity of the ubiquitin and Ubl proteases. Cell Res. 26, 441–456.

Rouge, L., Bainbridge, T.W., Kwok, M., Tong, R., Di Lello, P., Wertz, I.E., Maurer, T., Ernst, J.A., and Murray, J. (2016). Molecular understanding of USP7 substrate recognition and C-terminal activation. Structure 24, 1335–1345.

Sattler, M., Schleucher, J., and Griesinger, C. (1999). Heteronuclear multidimensional NMR experiments for the structure determination of proteins in solution employing pulsed field gradients. Prog. Nucl. Magn. Reson. Spectrosc. *34*, 93–158.

Song, M.S., Salmena, L., Carracedo, A., Egia, A., Lo-Coco, F., Teruya-Feldstein, J., and Pandolfi, P.P. (2008). The deubiquitinylation and localization of PTEN are regulated by a HAUSP-PML network. Nature *455*, 813–817.

Vranken, W.F., Boucher, W., Stevens, T.J., Fogh, R.H., Pajon, A., Llinas, M., Ulrich, E.L., Markley, J.L., Ionides, J., and Laue, E.D. (2005). The CCPN data model for NMR spectroscopy: development of a software pipeline. Proteins 69, 687–696

Weinstock, J., Wu, J., Cao, P., Kingsbury, W.D., McDermott, J.L., Kodrasov, M.P., McKelvey, D.M., Suresh Kumar, K.G., Goldenberg, S.J., Mattern, M.R., et al. (2012). Selective dual inhibitors of the cancer-related deubiquitylating proteases USP7 and USP47. ACS Med. Chem. Lett. 3, 789–792.

Zaman, M.M., Nomura, T., Takagi, T., Okamura, T., Jin, W., Shinagawa, T., Tanaka, Y., and Ishii, S. (2013). Ubiquitination-deubiquitination by the TRIM27-USP7 complex regulates tumor necrosis factor alpha-induced apoptosis. Mol. Cell. Biol. 33, 4971-4984.

Zapata, J.M., Pawlowski, K., Haas, E., Ware, C.F., Godzik, A., and Reed, J.C. (2001). A diverse family of proteins containing tumor necrosis factor receptorassociated factor domains. J. Biol. Chem. 276, 24242-24252.

Zhao, G.Y., Lin, Z.W., Lu, C.L., Gu, J., Yuan, Y.F., Xu, F.K., Liu, R.H., Ge, D., and Ding, J.Y. (2015). USP7 overexpression predicts a poor prognosis in lung squamous cell carcinoma and large cell carcinoma. Tumour Biol. 36, 1721-1729.

Zhu, Q., Sharma, N., He, J., Wani, G., and Wani, A.A. (2015). USP7 deubiquitinase promotes ubiquitin-dependent DNA damage signaling by stabilizing RNF168. Cell Cycle 14, 1413-1425.

Zlatanou, A., Sabbioneda, S., Miller, E.S., Greenwalt, A., Aggathanggelou, A., Maurice, M.M., Lehmann, A.R., Stankovic, T., Reverdy, C., Colland, F., et al. (2015). USP7 is essential for maintaining Rad18 stability and DNA damage tolerance. Oncogene 35, 965-976.

# **STAR**\***METHODS**

# **KEY RESOURCES TABLE**

REAGENT or RESOURCE	SOURCE	IDENTIFIER
Antibodies		
USP7	Progenra	N/A
DNMT1	Cell Signaling	Cat# 5032S; RRID: AB_10548197
HDM2	Santa Cruz	Cat# sc-965; RRID: AB_627920
UHRF1	Santa Cruz	Cat# sc-166898; RRID: AB_10610641
Actin	Sigma	Cat# A2228; RRID: AB_476697
Bacterial and Virus Strains	·	
Escherichia coli BL21(DE3)	EMD Millipore	Cat# 70235
Escherichia coli Rosetta 2(DE3)pLysS	EMD Millipore	Cat# 71401
Chemicals, Peptides, and Recombinant Proteins	Pro-	
222077	Calbiochem	Cat# 662142
P50429	Millipore	Cat# 662143
30423	Progenra	N/A
PR-619	LifeSensors	Cat# SI9619
Cycloheximide	Sigma	Cat# C7698
Jb-VME	LifeSensors	Cat# SI240
JSP7 (208-560)	This paper	N/A
His-SUMO-USP7 (208-560)	This paper  This paper	N/A
· '		N/A
His-FLAG -USP7 (208-560)	This paper	IV/A
Critical Commercial Assays	14.0	0.111 PD1001
Jb-CHOP2 reporter assays	LifeSensors	Cat# PR1001
CL	Millipore	Cat# WBKLS0500
ECL	Pierce	Cat# 34080
Deposited Data		
Backbone <sup>1</sup> H, <sup>13</sup> C and <sup>15</sup> N chemical shift	BMRB	26951
assignments for USP7 catalytic domain		
Experimental Models: Cell Lines		
Human: T lymphocyte cell line Jurkat (p53 <sup>MUT</sup> )	ATCC	Cat# TIB-152 <sup>TM</sup>
Human: HEK293T	ATCC	Cat# CRL-1573 <sup>™</sup>
Human: colorectal cancer HCT116 (p53 <sup>WT</sup> )	ATCC	Cat# CCL-247 <sup>™</sup>
Digonucleotides		
JSP7-208BsmBI-F: gatccgtctctaggtaagaag	Eurofins Genomics	Custom synthesis
cacacaggctacgt		
JSP7-560BsmBIXhoR: gatccgtctcctcgagt	Eurofins Genomics	Custom synthesis
eatteetgeegeteetteeget		
JSP7-208BsmBIXbaF: gatccgtctctctagaaa	Eurofins Genomics	Custom synthesis
gaagcacacaggctacgt		
JSP7-560BsmBINotR: gatccgtctccggccgct	Eurofins Genomics	Custom synthesis
eatteetgeegeteetteeget		
Khol-His10insertF: tcgagatgggtcaccatcacc lccatcaccatcatcatgggc	Eurofins Genomics	Custom synthesis
(hol-His10insertR: tcgagcccgtgatgatgatggtg	Eurofins Genomics	Custom synthesis
atggtggtgatggtgacccatc		,
JSP7-C223A-QC-F: gaatcagggagcgactgcttac	IDT Technologies	Custom synthesis
atgaacagcctgc		
JSP7-C223A-QC-R: gcaggctgttcatgtaagcagtc	IDT Technologies	Custom synthesis
geteeetgatte		

(Continued on next page)

Continued		
REAGENT or RESOURCE	SOURCE	IDENTIFIER
Recombinant DNA		
Plasmid: pET28a-LIC-USP7 (208-560)	SGC Toronto	N/A
Plasmid: pET24-6xHis-Smt3-USP7 (208-560)	This paper	N/A
Plasmid: pEF-10xHis-3xFLAG-USP7 (208-560)	This paper	N/A
Software and Algorithms		
NMRPipe	Delaglio et al., 1995	https://spin.niddk.nih.gov/bax/ software/NMRPipe/
CcpNmr Analysis	Vranken et al., 2005	http://www.ccpn.ac.uk/v2-software/ software/analysis
SciDAVis	N/A	http://scidavis.sourceforge.net/
Thermo Scientific Protein Deconvolution 4.0	Thermo Scientific	N/A
MASCOT Distiller	Matrix Science	http://www.matrixscience.com/ distiller.html
ICM-Pro	Molsoft	http://www.molsoft.com/ icm_pro.html
Chimera UCSF	Resource for Biocomputing, Visualization, and Informatics at the UCSF	http://www.rbvi.ucsf.edu/chimera
PROMALS3D	Pei et al., 2008	http://prodata.swmed.edu/ promals3d/promals3d.php
ConSurf	Ashkenazy et al., 2010	http://consurf.tau.ac.il/2016/

## **CONTACT FOR REAGENT AND RESOURCE SHARING**

Further information and requests for resources and reagents should be directed to and will be fulfilled by the Lead Contact, Irina Bezsonova (bezsonova@uchc.edu).

# **EXPERIMANTAL MODEL AND SUBJECT DETAILS**

#### **Bacterial Strains**

E. coli strain BL21-(DE3) was used to express USP7 (208-560) for NMR studies. USP7 catalytic domain used for in vitro experiments was purified from E. coli strain Rosetta 2(DE3)pLysS.

#### **Cell Lines**

Human T lymphocyte cell line Jurkat (p53<sup>MUT</sup>) was maintained in Roswell Park Memorial Institute (RPMI) 1640 Medium, supplemented with 10% FBS (Biowest) and 2 mM L-glutamine (Gibco), and 50 units/mL penicillin/streptomycin (Gibco). Human colorectal cancer HCT116 (p53<sup>WT</sup>) cell line and HEK293T cell line were maintained in Dulbecco's Modified Eagle Medium (DMEM) supplemented with 10% FBS 2 mM L-glutamine, and 50 units/mL penicillin/streptomycin.

### **METHOD DETAILS**

#### **USP7** Inhibitors

P22077 was purchased from Calbiochem. P50429 (Weinstock et al., 2012) was purchased from Millipore and synthesized at Progenra.

#### **Protein Expression and Purification**

USP7 sample used for NMR experiments: cDNA encoding the catalytic domain of the human USP7 (residues 208-560) was subcloned into pET28a-LIC Vector (Structural Genomics Consortium) downstream from an N-terminal 6xHis tag and a thrombin cleavage site. C223A mutation was introduced using site-directed mutagenesis. A  $^2$ H/ $^{13}$ C/ $^{15}$ N – labeled catalytic domain was expressed in *Escherichia coli* BL21 (DE3) strain grown at 37°C in 100% D<sub>2</sub>O-based M9 minimal medium supplemented with  $^{15}$ NH<sub>4</sub>Cl and  $^{13}$ C/ $^2$ H -glucose as the sole source for nitrogen and carbon respectively. Protein expression was induced at an OD<sub>600</sub>  $\sim$  0.8 by adding 1 mM IPTG. Cells were harvested after 16 hours of incubation at 20°C and lysed by sonication in extraction buffer containing 20 mM NaH<sub>2</sub>PO<sub>4</sub>, 250 mM NaCl, 10 mM imidazole, pH 7.4. Cell lysates were clarified by centrifugation at 15000 rpm for 45 min and applied to a Ni-NTA resin (Thermo Scientific). Recombinant protein was eluted with extraction buffer containing 250 mM imidazole. Following

thrombin digestion to remove the 6xHis-tag, catalytic domain was additionally purified by size exclusion chromatography using HiLoad Superdex 200 column (GE Healthcare) in sample buffer containing 20 mM Tris-HCl, 100 mM NaCl, 2 mM DTT, pH 7.5. For NMR experiments the protein sample additionally contained 10% D<sub>2</sub>O.

Catalytic domain of human USP7 (208-560) used for *in vitro* compound adduct formation study was sub-cloned into Bsal/Xholdigested pET24-6xHis-Smt3 vector (Malakhov et al., 2004). This bacterial-expression construct encoded a fusion protein with N-terminal 6xHis and SUMO tags, protein expression was performed in *Escherichia coli* strain Rosetta 2(DE3)pLysS by induction with 0.2 mM IPTG at 18°C overnight, and purification was achieved using Ni-NTA chromatography.

Catalytic domain of human USP7 (208-560) used for *in cells* (HEK293T) compound adduct formation study was sub-cloned into Xbal/Notl-digested pEF-3xFLAG-10xHis vector. This mammalian-expression construct of USP7 core encoded an N-terminally 3xFLAG-10xHis-tagged protein, expressed constitutively by the EF1 alpha promoter, and protein was purified through FLAG and His tags double affinity purification.

#### **NMR Spectroscopy**

All NMR data including spectra for backbone resonance assignment and chemical shift perturbation experiments were collected on 800 MHz (<sup>1</sup>H) Agilent VNMRS spectrometer equipped with cryoprobe at 30°C. The data were processed with NMRPipe (Delaglio et al., 1995) and analyzed with CcpNmr Analysis (Vranken et al., 2005). NMR experiments collected for backbone resonance assignment of the USP7 catalytic core included standard 2D <sup>1</sup>H-<sup>15</sup>N TROSY-HSQC, TROSY-based 3D HNCA, HNCOCA, HNCOC, HNCACO, HNCACB and <sup>15</sup>N-edited NOESY-HSQC (Pervushin et al., 1997; Sattler et al., 1999). To assess ubiquitin binding, unlabeled ubiquitin was gradually added to 0.3 mM <sup>2</sup>H/<sup>13</sup>C/<sup>15</sup>N – labeled catalytic domain of USP7 at ratios of up to 1:3 (protein to substrate). To monitor interactions of USP7 with its inhibitors, compounds P22077 or P50429 were dissolved in 100% DMSO and gradually added to 0.42 mM <sup>2</sup>H/<sup>13</sup>C/<sup>15</sup>N – labeled catalytic domain up to 1:5 protein-to-inhibitor ratio and final DMSO concentration of 5%. In all experiments changes in chemical shifts were monitored by acquiring 2D <sup>1</sup>H-<sup>15</sup>N TROSY spectra. During inhibitor binding experiments a spectrum of the free catalytic domain in sample buffer additionally containing 5% DMSO was used as a reference spectrum.

For USP7 catalytic core – ubiquitin complex observed frequency perturbations for each amino acid residue were calculated using combined shift change of the amide nitrogen and proton  $\Delta\omega_{obs} = (\Delta\omega_N^2 + \Delta\omega_H^2)^{1/2}$ , where  $\Delta\omega_N$  and  $\Delta\omega_H$  are <sup>15</sup>N and <sup>1</sup>H frequency differences between free and bound states in Hz. The dissociation constant for the complex of the catalytic domain with ubiquitin  $K_D = [P][L]/[PL]$  (where [P], [L] and [PL] are concentrations of the free protein, free substrate and the complex respectively) was extracted by nonlinear least-square fitting of global chemical shift change plotted versus ligand concentration using the following equation:

$$\Delta\omega_{obs} = \Delta\omega_{max}\frac{\left(\mathcal{K}_{D} + [L]_{t} + [P]_{t}\right) - \sqrt{\left(\left[P\right]_{t} + \left[L\right]_{t} + \mathcal{K}_{D}\right)^{2} - 4[P]_{t}[L]_{t}}}{2[P]_{t}}$$

where [P]<sub>t</sub> and [L]<sub>t</sub> are the total protein and ligand concentrations and  $\Delta\omega_{max}$  is chemical shift difference at saturation. A total of 199 assigned, well resolved non-overlapped peaks were used for the analysis. The titration data analysis was performed using SciDAVis. Figures depicting mapping of NMR data onto protein structures were prepared using Chimera UCSF (Pettersen et al., 2004) and ICM-Pro (Molsoft).

# **Mass Spectrometry**

Samples used for intact mass determination (Figure S4A) and LC-MS/MS (Figures 3B and 3C) were prepared by incubating 300  $\mu g$  of the purified catalytic domain with either 5-fold molar excess of P22077 or P50429 in the sample buffer containing 5% DMSO, or with vehicle (5% DMSO) for ~24 hours at room temperature. Following incubation, the protein samples were dialyzed in water to wash out salts and small molecules excess. To determine the intact mass of the USP7 catalytic core and its complexes with inhibitors, samples (~100  $\mu g$ , 30  $\mu$ l) were mixed with 200  $\mu$ l of 50% methanol containing 0.1% formic acid and analyzed by direct infusion on a Thermo Scientific Orbitrap Fusion Tribrid mass spectrometer. The instrument was operated in Intact Protein mode with an ion routing multipole pressure of 1mTorr. Spectra were acquired at 120K and 240K resolution. The isotopically resolved data were processed using Thermo Scientific Protein Deconvolution 4.0 software. Samples used for LC-MS experiments shown in Figures 3A and S4D were prepared by incubating 300  $\mu$ g of the purified WT and C223A catalytic domain with 20-fold molar excess of either P22077 or P50429 with 2% DMSO for 4 hours at room temperature and analyzed at Progenra using Agilent 6230 TOF LC/MS system. For MS analysis of *in cells* compound adduct formation (Figure 5C), HEK293T cells expressing WT or C223A 3xFLAG-10xHis-USP7 catalytic domain were treated with DMSO, 30  $\mu$ M P22077, or 30  $\mu$ M P50429 for 4 hours. Followed purification, 600 ng of the protein was analyzed using Agilent 6230 TOF LC/MS system.

For LC-MS/MS, the intact protein samples (~10 µg) were dried using SpeedVac prior to dissolving and denaturing in 8 M urea, 0.4 M ammonium bicarbonate. The urea concentration was adjusted to 2 M by the addition of water, and the proteins were digested with trypsin (Promega) at 37°C for 16 hours. Samples were desalted using a C18 Ultra microspin column (The Nest Group) and peptides were eluted with 80% acetonitrile containing 0.1% trifluoroacetic acid (TFA), then dried and reconstituted in 7% formic acid/ 0.1% TFA, then diluted with additional 0.1% TFA to a final protein concentration of 0.01 µg/µl. LC-MS/MS analysis was performed

on a Thermo Scientific Q Exactive Plus equipped with a Waters nanoAcquity UPLC system using a Waters Symmetry® C18 180μm x 20mm trap column and a ACQUITY UPLC PST (BEH) C18 nanoACQUITY Column (1.7 μm, 75 μm x 250 mm) for peptide separation. Trapping was done at flow rate of 5 μl/min in 97% Buffer A (100% water, 0.1% formic acid) for 3 min. Peptide separation was performed at 330 nl/min with the following gradient of Buffer B (100% acetonitrile, 0.1% formic acid) in Buffer A for 90 minutes: 3% B at initial conditions; 5% B at 1 minute; 35% B at 50 minutes; 50% B at 60 minutes; 90% B at 65-70; and back to initial conditions at 71 minutes. MS was acquired in profile mode over the 300-1,700 m/z range using 1 microscan; 70,000 resolution; AGC target of 3E6; and a full max ion time of 45 ms. MS/MS was acquired in centroid mode using 1 microscan; 17,500 resolution; AGC target of 1E5; full max ion time of 100 ms; 1.7 m/z isolation window; normalized collision energy of 28; and 200-2,000 m/z scan range. Up to 20 MS/MS were collected per MS scan on species with an intensity threshold of 2E4, charge states 2-6, peptide match preferred, and dynamic exclusion set to 20 seconds. MASCOT Distiller software was used to generate peak lists which were searched against the UBP7\_HUMAN sequence as well as the Swiss-Protein database with taxonomy restricted to E. coli using the MASCOT algorithm (Matrix Science). Search parameters used were peptide mass tolerance of 10 ppm; MS/MS fragment tolerance of +0.25 Da; allow up to two missed cleavages; variable modification of methionine oxidation and custom modifications configured for the moieties added by the compounds.

#### **Protein - Ligand Docking**

Covalent docking of the complexes of USP7 catalytic domain with DUB inhibitors P22077 and P50429 was performed using ICM-Pro (Molsoft). ICM method uses Monte-Carlo simulations based global optimization of flexible ligand position in the space of grid potential energy maps calculated for a protein receptor (Neves et al., 2012). Chemical reactions for both of the compounds were sketched manually. Covalent adducts were identified based on MS results and represented products of the chemical reactions. C223 was chosen as the modified residue. The highest resolution X-Ray structure of USP7 catalytic core was used (PDB: 4M5W) (Molland et al., 2014). Structures with the lowest predicted ICM scoring function accounting for ligand size, protein - ligand van der Waals interactions, conformational changes, changes in solvation electrostatic energy and hydrophobic free energy gain are shown in Figures 6A and 6B.

#### **Immunoprecipitation and DUB Activity Measurements**

Immunoprecipitation and measurement of USP7 activity were performed as reported previously (Chauhan et al., 2012) with slight modifications. Briefly, Jurkat cells treated with DMSO or USP7 inhibitors were washed with ice cold PBS and lysed using NP40 lysis buffer (50 mM Tris-HCl, pH 7.5, 150 mM NaCl, 1% (v/v) NP40, 10% (v/v) Glycerol, 1 mM PMSF) and pre-cleared using 30 µl of protein G-sepharose (Invitrogen) for 1 hour at 4°C. 500 µg of pre-cleared cell lysates were incubated with Protein G sepharose beads pre-loaded with 0.5 μg of anti-USP7 antibody (Progenra) for 1 hour. Beads were washed twice with lysis buffer containing 2 mM β-mercaptoethanol and USP7 activity was determined using Ub-CHOP2 reporter assays (LifeSensors). DMSO treated cell lysates were incubated with beads alone for control. 5 μl of beads from immunoprecipitation was analyzed by Western blotting with anti-USP7 antibody to determine relative levels of USP7.

# Irreversible Inhibition of Endogenous USP7 in HCT116 Cells

HCT116 cells were pre-treated with either DMSO, P22077 or P50429 for 4 hours, and then the free inhibitors were washed out with 1X PBS. Cells were cultured with fresh medium for 24 hours in the presence or absence of Cycloheximide (CHX), to block new protein synthesis. Endogenous USP7 was then isolated by immunoprecipitation for quantification of catalytic activity using Ub-CHOP2 reporter assay (LifeSensors).

#### **Western Blotting**

Jurkat cells were treated with USP7 inhibitors for 24 hours with indicated doses, harvested and washed once with ice-cold PBS. Cell pellets were lysed using modified RIPA lysis buffer (50 mM Tris-HCl, pH 7.5, 150 mM NaCl, 1% NP40, 1% Sodium deoxycholate, 2 mM EDTA, 10% Glycerol, Protease inhibitor cocktail (Sigma, 1:500), 50 μM PR-619 (Pan DUB inhibitor, LifeSensors). Protein estimation was carried out using the Bradford method (Bio-Rad). 25 µg of cell lysates were separated on 10% SDS-PAGE gel, transferred to PVDF membrane and probed with primary antibodies against DNMT1 (Cell Signaling) HDM2 (Santa Cruz), UHRF1 (Santa Cruz) and Actin (Sigma). Blots were developed using Millipore ECL or Pierce ECL depending on the sensitivity requirements and images were captured and quantified using LI-COR Odyssey Fc imaging system. For repeated analysis of Western blots, membranes were stripped using Restore Western Blot Stripping buffer (ThermoFisher).

#### **Ub-VME** based **USP7** Activity Assay

HEK293T cells expressing WT or C223A USP7 core were pre-treated with either 30 μM of the inhibitors or DMSO for 4 hours. Cells were washed once with PBS, harvested and lysed in 1% NP40 lysis buffer (50 mM Tris-HCl, pH 7.5, 150 mM NaCl, 1% NP40, 10% Glycerol, 1 mM PMSF, 2 mM  $\beta$ -ME). 20  $\mu$ g of lysate per sample was used for the Ub-VME assay by incubating with Ub-VME at a final



concentration of 400 nM. Total reaction volume was 10  $\mu$ l. The reaction was performed at 37 °C for 30 min and stopped by addition of 2  $\mu$ l of 6X SDS sample buffer and boiling for 5 min. To determine the formation of USP7-Ub-VME complex the samples were subjected to SDS-PAGE electrophoresis, transfered to PVDF membrane, and blotted with USP7-specific antibody.

# **DATA AND SOFTWARE AVAILABILITY**

The backbone <sup>1</sup>H, <sup>13</sup>C and <sup>15</sup>N chemical shift assignments of USP7 catalytic domain have been deposited to BMRB under the accession number BMRB: 26951.